Accepted Manuscript

Discovery of a potent and highly selective transforming growth factor β receptor-associated kinase 1 (TAK1) inhibitor by structure based drug design (SBDD)

Terushige Muraoka, Mitsuaki Ide, Kenji Morikami, Machiko Irie, Mitsuaki Nakamura, Takaaki Miura, Takayuki Kamikawa, Masamichi Nishihara, Hirotaka Kashiwagi

PII: S0968-0896(16)30498-9
DOI: http://dx.doi.org/10.1016/j.bmc.2016.07.006
Reference: BMC 13119

To appear in: *Bioorganic & Medicinal Chemistry*

Received Date: 27 May 2016
Revised Date: 4 July 2016
Accepted Date: 5 July 2016

Please cite this article as: Muraoka, T., Ide, M., Morikami, K., Irie, M., Nakamura, M., Miura, T., Kamikawa, T., Nishihara, M., Kashiwagi, H., Discovery of a potent and highly selective transforming growth factor β receptor-associated kinase 1 (TAK1) inhibitor by structure based drug design (SBDD), *Bioorganic & Medicinal Chemistry* (2016), doi: http://dx.doi.org/10.1016/j.bmc.2016.07.006

Discovery of a potent and highly selective transforming growth factor β receptor-associated kinase 1 (TAK1) inhibitor by structure based drug design (SBDD).

Terushige Muraoka [a*], Mitsuaki Ide [a], Kenji Morikami [a], Machiko Irie [b], Mitsuaki Nakamura [b], Takaaki Miura [b], Takayuki Kamikawa [b], Masamichi Nishihara [a] and Hirotaka Kashiwagi [a]

[a] *Research Division, Chugai Pharmaceutical Co,. Ltd., 1-135 Komakado, Gotemba, Shizuoka 412-8513, Japan*

[b] *Research Division, Chugai Pharmaceutical Co., Ltd., 200 Kajiwara, Kamakura, Kanagawa 247-8530, Japan*

*Corresponding author. Tel.: +81 0550 87 6742; fax: +81 0550 87 5326

E-mail address: muraokatrs@chugai-pharm.co.jp (T. Muraoka).

Key words: TAK1, SBDD, inhibitor, kinase selectivity

Abstract

A novel thienopyrimidinone analog was discovered as a potent and highly selective TAK1 inhibitor using the SBDD approach. TAK1 plays a key role in inflammatory and immune signaling, so TAK1 is considered to be an attractive molecular target for the treatment of human diseases (inflammatory disease, cancer, etc.). After the hit compound had been obtained, our modifications successfully increased TAK1 inhibitory activity and solubility, but metabolic stability was still unsatisfactory. To improve metabolic stability, we conducted metabolic identification. Although the obtained metabolite was fortunately a potent TAK1 inhibitor, its kinase selectivity was low. Subsequently, to achieve high kinase selectivity, we used SBDD to follow two strategies: one targeting unique amino acid residues in TAK1, especially the combination of Ser111 and Asn114; the other decreasing the interaction with Tyr106 at the hinge position in TAK1. As expected, our designed compound showed an excellent kinase selectivity profile in both an in-house and a commercially available panel assay of over 420 kinases and also retained its potent TAK1 inhibitory activity (TAK1 IC_{50}=11 nM).

1. Introduction

Transforming growth factor β receptor-associated kinase 1 (TAK1) is a serine/threonine kinase that plays a key role in inflammatory and immune signaling. TAK1 was first discovered by Matsumoto et al. as a member of the mitogen-activated kinase kinase kinase (MAP3K) family activated by transforming growth factor-β (TGF-β),[1] and since then has been elucidated as a mediator of multiple cytokines such as TNF-α, IL-1, LPS, etc.[2-4] TAK1 exerts its activity only when it forms complexes with its activator proteins TAB1 and TAB2 or TAB3.[5-7] TAB1 binds to TAK1 at the N-terminal domain, while either TAB2 or TAB3 binds to TAK1 at the C-terminal domain. TAK1 phosphorylates downstream kinases, such as the mitogen-activated kinase kinase (MKK) family (MKK3/4/6/7), p38, c-Jun N-terminal kinase (JNK), and the IκB kinase (IKK) family (IKKα, IKKβ, and NEMO), to activate transcription factors, such as activation protein-1 (AP-1) and nuclear factor-κB (NF-κB), which regulate stress response, immunity, inflammation, and cancer signaling. Indeed, p38 and IKK

have been developed as targets for rheumatoid arthritis and airway inflammation,[8] and systemic administration of TAK1 siRNA particles has been shown to alleviate inflammation in a mouse model of immune-mediated inflammatory disorder.[9] In summary, TAK1 is considered to be an attractive molecular target for the treatment of human diseases (inflammatory disease, cancer, etc.).

It is important that compounds designed as kinase inhibitors have a good kinase selectivity profile because inhibiting particular kinases carries the risk of adverse effects. For example, inhibiting KIT and KDR is related to bone marrow suppression and hypertension, respectively.[10, 11] Additionally, although FLT3 is an attractive target for acute myelogenous leukemia and acute lymphocytic leukemia, it plays a key role in the normal development of stem cells and the immune system in hematopoiesis;[12] therefore, we considered that FLT3 inhibition should be avoided, especially in chronic diseases. Of over 500 kinases in human[13] that maintain the functions of cells, it is not completely clear which kinase inhibition causes an adverse event. A further reason why compounds need to have high kinase selectivity is to elucidate the mode of action more easily. Even if a multi kinase inhibitor achieves the desired phenotype, we are still not able to tell whether its desired effect is a consequence of target inhibition or not.

Several TAK1 inhibitors have been reported previously (Figure 1)[14]. 5Z-7-oxazeaenol **1**[15, 16] and epoxyquinol B **2**[17, 18], the natural products known as irreversible inhibitors, are unselective kinase inhibitors that nevertheless have potent TAK1 inhibitory activity. Thiophene carboxamide **3**[19] and oxindole **4**[20] also have potent TAK1 inhibitory activity, but their selectivity data has not been reported. Although the TAK1 IC_{50} of imidazopyridazine **5**[21] is 8.0 nM, a kinase panel showed that it had IC_{50} < 100 nM to 10/30 kinases other than TAK1, so we consider its TAK1 selectivity to be low. The recently discovered TAK1 inhibitor, 7-aminofuro[2,3-c]pyridine **6**[22, 23] (OSI Pharmaceuticals), showed >50% inhibition for 4/192 kinases (FLT3, HGK, MAP4K5, and MINK1) at fifty times the concentration of TAK1 K*i*, so can be considered relatively selective, but as explained above its FLT3 inhibitory activity would be undesirable. Whereas compounds **1**~**6**, which bind TAK1 in the DFG-in conformation, are known as type I inhibitors, Pfizer has reported the first type II inhibitor, pyrazole urea **7**[24], which binds TAK1 in the DFG-out conformation. According to the preliminary study, TAK1 inhibitory activity and selectivity of compound **7** are not sufficient.

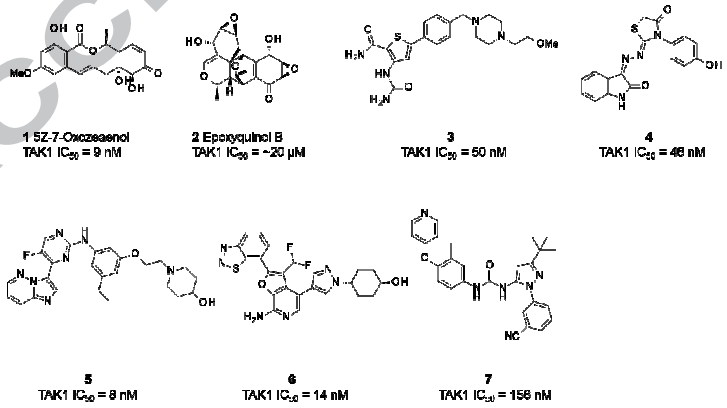

Figure 1. Structure of previously reported TAK1 inhibitors (**1**-**7**)

Here, we report the discovery of novel potent and selective TAK1 inhibitor **12** that possesses a thienopyrimidinone moiety as a scaffold (Figure 2). Our starting compound **8** was obtained from two focused libraries selected from in-house compounds; the first library was selected from inhibitors against five kinases that either had similar amino acid sequences or for which cross activity against TAK1 kinase was strongly predicted by the existing patent information, and the second library included kinase inhibitors with excellent kinase selectivity profile (fewer than five kinases with Kd < 1 μM) as characterized by KinomeScan™ (DiscoverRX, an in vitro binding panel assay system). We assayed their binding activity to TAK1 with SPR (manuscript in preparation) and refer to the use of these focused libraries as the "chemogenomics approach". Compound **8**, which showed the expected good TAK1 selectivity profile but had extremely low solubility, was then modified to increase TAK1 inhibitory activity and solubility, which resulted in compounds **11c** and **11i** with potent TAK1 inhibitory activity. These compounds were then further modified to improve their kinase selectivity profile by fully utilizing the information from the X-ray structures of the inhibitor-TAK1 complexes. As a result, we were able to discover compound **12** with both potent TAK1 inhibitory activity (TAK1 IC_{50}=11 nM) and high kinase selectivity. The in-house panel data of 38 kinases, including FLT3, showed no significant inhibition (IC_{50} > 10μM) other than that against TAK1. More significantly, in a KinomeScan™ panel of 442 kinases, **12** showed a 50% binding inhibition larger than 1.0 μM against as few as four kinases, one of which was TAK1.

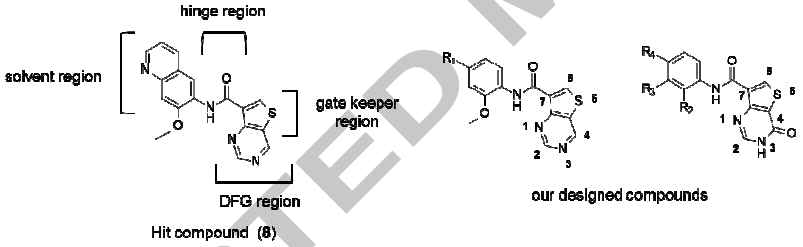

9a : R_1 = (N-methyl piperazine)C=O
9b : R_1 = (N-methyl piperazine)$CH_2CH_2CH_2NHC$=O
9c : R_1 = N-methyl piperazine
10 : R_2 = OMe, R_3 = H, R_4 = (N-methyl piperazine)$CH_2CH_2CH_2NHC$=O
11a : R_2 = Me, R_3 = H, R_4 = (N-methyl piperazine)C=O
11b : R_2 = iPr, R_3 = H, R_4 = (N-methyl piperazine)C=O
11c : R_2 = Ph, R_3 = H, R_4 = (N-methyl piperazine)C=O
11d : R_2 = cyclohexyl, R_3 = H, R_4 = (N-methyl piperazine)C=O
11e : R_2 = F, R_3 = H, R_4 = (N-methyl piperazine)C=O
11f : R_2 = Cl, R_3 = H, R_4 = (N-methyl piperazine)C=O
11g : R_2 = Br, R_3 = H, R_4 = (N-methyl piperazine)C=O
11h : R_2 = OMe, R_3 = H, R_4 = (N-methyl piperazine)C=O
11i : R_2 = OiPr, R_3 = H, R_4 = (N-methyl piperazine)C=O
11j : R_2 = hexafluoroisopropoxy, R_3 = H, R_4 = (N-methyl piperazine)C=O
11k : R_2 = NMe_2, R_3 = H, R_4 = (N-methyl piperazine)C=O
11l : R_2 = NEt(Me), R_3 = H, R_4 = (N-methyl piperazine)C=O
12 : R_2 = OiPr, R_3 = (N-methyl piperazine)C=O, R_4 = H

Figure 2. Structure of Hit compound (**8**) and our designed TAK1 inhibitors.

2. Chemistry

The synthesis of thienopyimidine **16** and thienopyrimidinone **19** is shown in Scheme 1[25]. The common intermediate **14** of both **16** and **19** was synthesized from commercially available thiophene **13** in moderate yield (2 steps 72%). The hydrogenation of **14** with palladium hydroxide generated **15** in 94% yield.

Subsequently, dibromination of **15** at the benzylic position obtained the aryl aldehyde, which was then subjected to oxidation reaction to give the desired thienopyrimidine **16** (3 steps 58%). As for the synthesis of thienopyrimidinone **19**, compound **17** was obtained first by dibromination of **14**. After the generation of trimethoxy compound by treating **17** with methanol, aldehyde **18** was obtained under acidic condition. Finally, the oxidation of the aldehyde gave the desired thienopyrimidinone **19** in good yield (3 steps 75%).

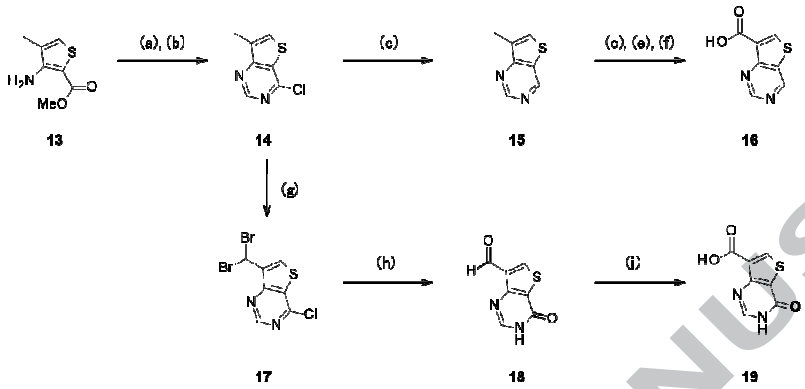

Scheme 1. Synthesis of thienopyrimidine **16** and thienopyrimidinone **19**. Reagents and conditions: (a) Formamide, 150 °C; (b) $POCl_3$, 100 °C, 2 steps 72%; (c) H_2 gas (1.0 atm), 20% $Pd(OH)_2/C$, Et_3N, EtOAc/*i*-PrOH = 5/1, room temp. 94%; (d) NBS, benzoyl peroxide, CCl_4, reflux; (e) Pyridine, H_2O, 100 °C; (f) $NaClO_2$, sulfamic acid, acetone, H_2O, 40 °C, 3 steps 58%; (g) NBS, AIBN, CCl_4, reflux; (h) MeOH, 70 °C and then 5N HCl aq., THF, 60 °C.; (i) $NaClO_2$, sulfamic acid, acetone, H_2O, room temp., 3 steps 71%.

The synthesis of thienopyrimidine analogs (**9a**-**9c**) by amidation is shown in Scheme 2. Aniline parts (**20a-20c**) were prepared using a commercially available substituted benzene **21** or **22** in good yield. Thienopyrimidinone analogs **10**, **11a-l**, and **12** were synthesized by a similar method as the thienopyrimidine analogs **9a-c** (Scheme 3). The preparation method of aniline parts is shown in Supplementary Scheme 1.

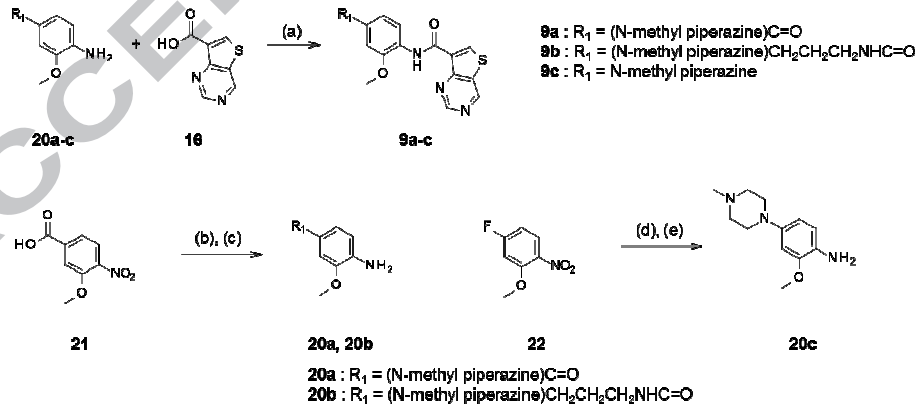

Scheme 2. Synthesis of thienopyrimidine analog. Reagents and conditions : (a) HATU, DIPEA, **20a-c**, acetonitrile; (b) amine, HATU, DIPEA, DCM; (C) H_2, 10% Pd/C, ethanol; (d) N-methyl piperazine, Et_3N, DMA; (e) H_2, 10% Pd/C, methanol.

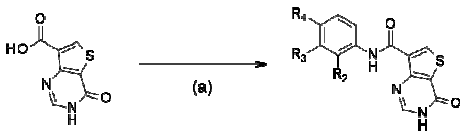

10 : R_2 = OMe, R_3 = H, R_4 = (N-methyl piperazine)$CH_2CH_2CH_2NHC$=O

11a : R_2 = Me, R_3 = H, R_4 = (N-methyl piperazine)C=O

11b : R_2 = iPr, R_3 = H, R_4 = (N-methyl piperazine)C=O

11c : R_2 = Ph, R_3 = H, R_4 = (N-methyl piperazine)C=O

11d : R_2 = cyclohexyl, R_3 = H, R_4 = (N-methyl piperazine)C=O

11e : R_2 = F, R_3 = H, R_4 = (N-methyl piperazine)C=O

11f : R_2 = Cl, R_3 = H, R_4 = (N-methyl piperazine)C=O

11g : R_2 = Br, R_3 = H, R_4 = (N-methyl piperazine)C=O

11h : R_2 = OMe, R_3 = H, R_4 = (N-methyl piperazine)C=O

11i : R_2 = OiPr, R_3 = H, R_4 = (N-methyl piperazine)C=O

11j : R_2 = hexafluoroisopropoxy, R_3 = H, R_4 = (N-methyl piperazine)C=O

11k : R_2 = NMe_2, R_3 = H, R_4 = (N-methyl piperazine)C=O

11l : R_2 = NEt(Me), R_3 = H, R_4 = (N-methyl piperazine)C=O

12 : R_2 = OiPr, R_3 = (N-methyl piperazine)C=O, R_4 = H

Scheme 3. Synthesis of thienopyrimidinone analogs. : (a) HATU, DIPEA, aniline, acetonitrile.

3. Results and discussion

We found the hit compound **8** by SPR screening but its low solubility made it impossible to evaluate TAK1 inhibitory activity at more than 1.0 μM (37% inhibition at 1.0 μM). Indeed, its solubility measured by fasted state simulated intestinal fluid (FaSSIF) or phosphate buffer (PPB) at pH 6.5 was less than 3.0 μg/mL because of its planar structure[26].

First, the quinoline ring of hit compound **8** was substituted for the benzene ring bearing a hydrophilic group, to improve the solubility. The dissolution of the resultant compounds **9a-c** was much improved both in FaSSIF and in PPB, and **9b** also exhibited TAK1 inhibitory activity three times more potent than the hit compound **8**, but metabolic stability, especially in mouse microsomes, was low compared to human (Table 1).

Table 1. TAK1 inhibitory activity and physicochemical parameters of HTS hit compound (**8**) and thienopyrimidine analogs (**9a-9c**)

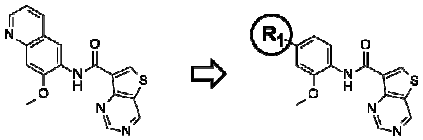

Hit compound **8**

compound	R_1	Kinase IC_{50} (μM)	FaSSIF(PPB) (μg/mL)	CLint(μL/min/mg)	
				human	mouse
Hit compound **8**	-	37% inhibition @ 1μM	**< 3 (< 3)**	-	-
9a		1.6	**312 (293)**	26	-
9b		**0.26**	**420 (377)**	21	80
9c		1.3	**351 (353)**	11	-

In order to identify the metabolically labile site of **9b**, its metabolites were structurally analyzed, particularly one main metabolite observed in both human and mouse liver microsomes, metabolite **10**, which possessed a potent TAK1 inhibitory activity (IC_{50}=13 nM) (Figure 3(a)). Because we discovered this metabolite was generated in liver cytosol, the main metabolite **10** was isolated using **9b** in mouse liver cytosol to determine the structure by LC-MS and NMR, which showed that an oxidation reaction at 4 position of the thienopyrimidine ring of **9b** had occurred. Metabolite **10** was found to be a potent TAK1 inhibitor (IC_{50}=13 nM), so we used X-ray analysis on an opportunely obtained crystal structure of metabolite **10** in TAK1 to understand this increased TAK1 inhibitory activity.

The X-ray crystal structure showed **10** was binding to TAK1 in the DFG-in conformation known as a type I inhibitor (Figure 3(b)). Focusing on how differences between **9b** and **10** increased TAK1 inhibitory activity, we found that the critical difference was a carbonyl group of thienopyrimidinone located near the DFG loop and the gatekeeper of TAK1. The X-ray information revealed that the distance from this carbonyl group to crystal water was 2.9 Å and the distance from the crystal water to the backbone amide NH of Asp175 (DFG) was 2.9 Å. In other words, this carbonyl group of thienopyrimidinone has tight interactions with the backbone amide NH of Asp175 by hydrogen bonding via a crystal water. In addition, we argue that this carbonyl group also has a tight interaction with the side chain of Glu77, though because this is not clear in the X-ray crystal structure, we confirmed that some derivatives with a thienopyrimidinone ring like compound **10** interacted with the side chain of Glu77 via this crystal water (PDB code: 5JGA and 5JGD). As a result of these tight interactions,

desirable effects on the potent inhibitory TAK1 activity of **10** were obtained in comparison to **9b**. Next, we elucidated another interaction between **10** and TAK1, with the distance from amide NH at 3-position of the thienopyrimidinone ring to the side chain of DFG Asp175 of 2.6 Å, and the distance from the S atom at 5-position of thienopyrimidinone to the side chain of gatekeeper Met104 of 4.0 Å, which meant that thienopyrimidinone of **10** had a tight interaction with DFG Asp175 by hydrogen bonding and a weak hydrophobic interaction with Met104. Subsequently, in the hinge position, the distance from an amide carbonyl group at 7-position of the thienopyrimidinone part of **10** to Ala107 was 2.7 Å, which created a hydrogen bonding interaction with TAK1 in this region. Finally, at N-methyl piperazine moiety located in the solvent region, no tight interaction was found. These interactions between **10** and TAK1, especially those between the carbonyl group of the thienopyrimidinone ring and TAK1 via crystal water, led to potent TAK1 inhibitory activity (IC_{50}=13 nM).

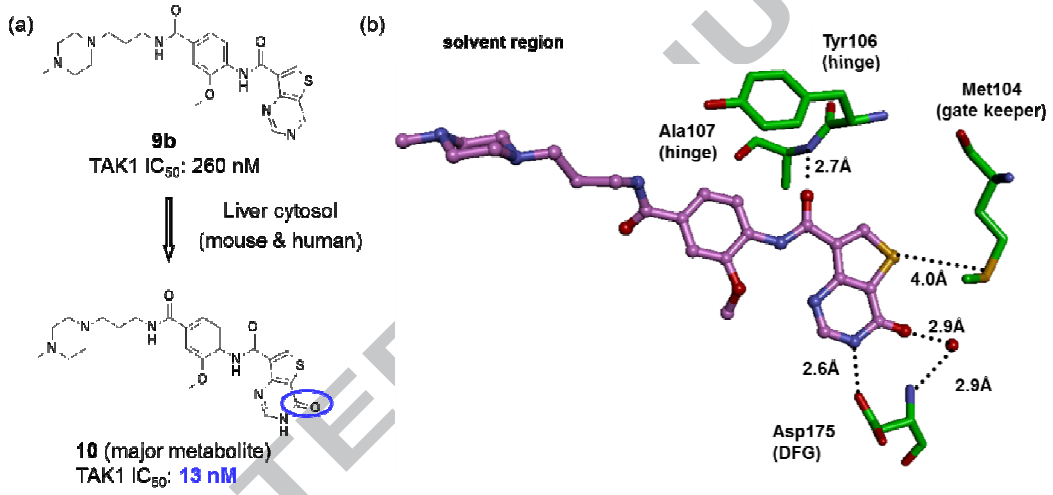

Figure 3. (a) Metabolic reaction of **9b** in liver cytosol. (b) X-ray crystal structure of **10** (metabolite of **9b**) in TAK1 (PDB code: 5JGB). **10** is shown as a ball and stick model colored by element type (C in magenta, O in red, N in blue, S in yellow). Amino acid residues of TAK1 that interact with compound **10** are shown as stick models colored by element type with the same colors, except for C in light green. A representative crystallographic water is depicted as a red sphere. The key interactions are depicted as dotted lines.

Subsequently, we explored the SAR of R_2 group (Table 2), which the X-ray crystal structure showed was located in the vicinity of hydrophobic amino acids Val42, Gly43, Gly45, Val50, Gly110, Pro160, and Leu163. Thus, we defined this region as hydrophobic and introduced a hydrophobic R_2 group in this region to enhance the interaction with TAK1. As for the linker connecting the benzene ring and R_2 groups, three different types (C-linker, O-linker and N-linker) were prepared to change the direction of the R_2 group, and halogen derivatives were also evaluated. In each case, the volume of the R_2 group was calculated while ignoring the hydrogen atoms. The tendency obtained with each linker type was very similar. As expected, TAK1 inhibitory

activity increased as the volume of the hydrophobic R_2 group increased; however, reduced TAK1 inhibitory activity was observed when the volume of the R_2 group was beyond the local maximum value of each linker type (Figure 4). Regarding the TAK1 inhibitory activity of C-linker derivatives **11a**-**11d**, **11c** had the most potent (2.3 nM); **11a**, which had insufficient occupancy in this hydrophobic region, showed the weakest (41 nM); while **11d**, which possessed the largest substituent, cyclohexane, was slightly weaker (6.7 nM) than **11c**. Halogen derivatives (**11e-11g**) and O-linker derivatives (**11h**-**11j**) had the same tendency as C-linker derivatives; chlorine derivative **11f** and *i*PrO derivative **11i** group were the most potent (5.8 nM and 3.0 nM, respectively); fluorine derivative **11e** (220 nM) and OMe derivative **11h** (15 nM) were the weakest, with insufficient volume of R_2 group; but **11g** (7.3 nM) and **11j** (5.2 nM), which possessed the largest substituent (a bromine and hexafluoroisopropoxy group), had slightly weaker activity than **11f** and **11i**, respectively. Regarding TAK1 inhibition of N-linker derivatives, **11k** with a dimethyl amino group was 5.0 nM, while **11l** with an ethyl methyl amino group was 9.3 nM; therefore, we estimated that the local maximum value of N-linker types would be below 65 $Å^3$ of volume. We considered that the difference in local maximum value of TAK1 inhibitory activity shown by each linker type depended on the difference in the direction of the benzene ring in R_2. Having discovered potent TAK1 inhibitors **11c** and **11i** (IC_{50}=2.3 nM and 3.0 nM, respectively), we evaluated the kinase selectivity of these compounds, but it was unfortunately low. The result of the in-house panel assay of 38 kinases showed that **11c** also had inhibitory activity below 1.0 μM against 14 kinases other than TAK1. In particular, **11c** had potent inhibitory activity against FLT3 (IC_{50}=5.4 nM), which we felt should be avoided, and **11i** also had the same tendency as **11c**. By exploiting the hydrophobic pocket, we had succeeded in finding TAK1 inhibitors as potent as **11c** and **11i**, but their kinase selectivity profile was rather compromised, presumably because the ATP sugar part occupied this pocket in TAK1 and the amino acid residues around this pocket are common to many kinases

Table 2. SAR table for TAK1 activity and calculated volume of R_2 group.

[a] calculated volume of side chain moiety (R_2 group) extracted from whole molecule.

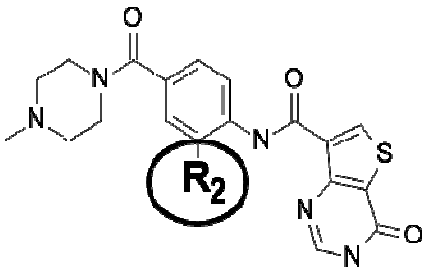

Compound	R_2	Kinase IC_{50} (nM)	Volume ($Å^3$)[a]
11a		41	27
11b		3.5	56
11c	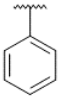	2.3	66
11d	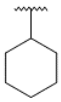	6.7	87
11e		220	12
11f		5.8	25
11g		7.3	27
11h		15	32
11i		3.0	64
11j	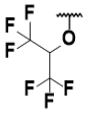	5.2	95
11k		5.0	52
11l		9.3	65

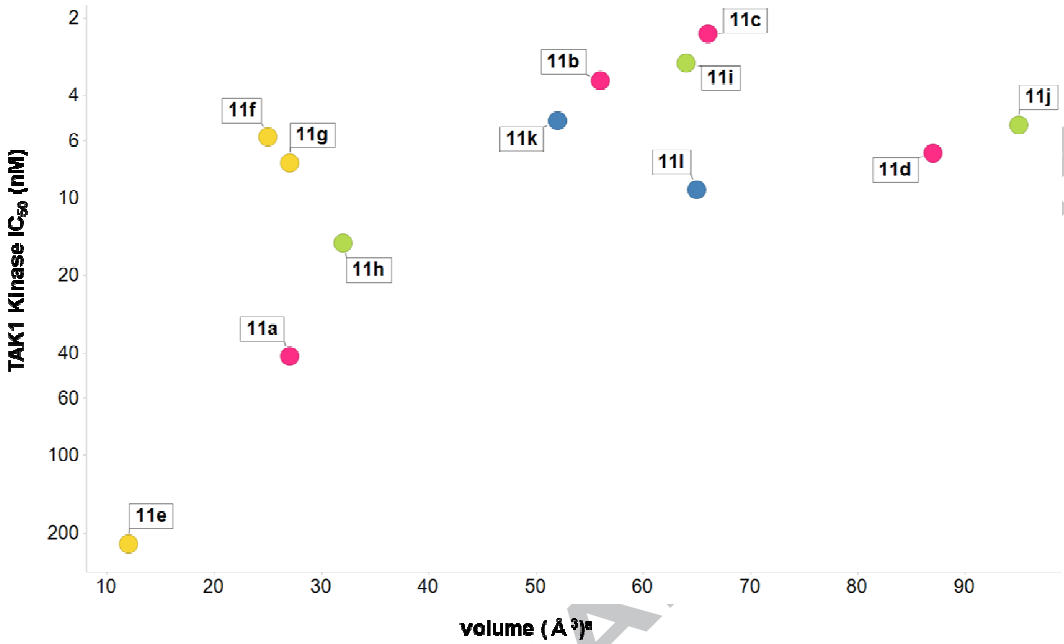

Figure 4. Relationship between TAK1 activity and volume of R_2 group in thienopyrimidinone analogs (**11a**-**11l**). (magenta: C-linker derivative, yellow: halogen derivative, light green: O-linker derivative, cyan: N-linker derivative)

[a] calculated volume of side chain moiety (R_2 group) extracted from whole molecule.

To improve the kinase selectivity of **11c** or **11i**, we adopted two strategies that utilized 3D structure information. The first one was to target specific amino acid residues in TAK1, especially the combination of Ser111 and Asn114, which was revealed to be very unique from a search of an in-house database constructed from literature on 490 kinases[13] (Figure 5 (b)). The second strategy was to reduce the interaction between the amide moiety located at R_4 position in the substituted benzene and Tyr106 at the hinge position in TAK1. For the first strategy, we made use of previous reports[22, 23] by OSI Pharmaceuticals in which Ser111 was targeted to obtain selectivity to TAK1 over Aurora B. Because Ser111 in TAK1 corresponds in Aurora B to the larger Glu161, they suggested that clashing with the Glu161 in Aurora B meant that their compound **6** was more selective to TAK1 than to Aurora B, but moderately selective to FLT3 (at fifty times the concentration of TAK1 K*i*, **6** showed > 50% FLT3 inhibition). We found that out of 490 kinases, position 111 was occupied by Ser in 115 kinases (as in TAK1), by Glu in 91 kinases (as in Aurora B), and by Asp in 161 kinases (as in FLT3). We considered that the difference between Asp and Glu made compound **6** more selective to Aurora than to FLT3, because the size of Asp is smaller than Glu, so compound **6** bumped less against FLT3. To obtain high TAK1 kinase selectivity, we focused on the combination of Ser111 and Asn114 in TAK1. As mentioned above, Ser is a fairly common amino acid residue, but only 20 kinases had Asn corresponding to the 114 position, as TAK1 does, and possessing both Ser and Asn at these positions is very rare and unique; in fact, only one kinase other

than TAK1, integrin-linked kinase (IIK), has this combination. From the X-ray information of compound **11c** in TAK1, the distance from the carbonyl group of R_4 group in the solvent region to Ser111 and Asn114 was 6.7 Å and 4.7 Å, respectively, which indicated that the compound had insufficient interaction against the area surrounding these TAK1 unique amino acids (Figure 5 (a)). We supposed that the desirable interaction with TAK1 at Ser111 and Asn114 would improve kinase selectivity.

For the second strategy, we did a similar search of 490 kinases for amino acid residues corresponding to Tyr106 in TAK1, and found that 198 have Tyr in this position, and additionally many kinases (304) have aromatic amino acid residues there. The X-ray structure of **11c** in TAK1 showed that the distance from the N-methyl piperazine ring at R_4 group to Tyr106 is 3.4 Å, which indicated a CH-π interaction[27] between **11c** and TAK1. We assumed that the same interaction between **11c** and other kinases exists, and that reduction of this interaction would improve kinase selectivity.

We designed compound **12** to adopt a simple but efficient plan that was able to achieve these two different strategies simultaneously. Specifically, N-methyl piperazine amide moiety at R_4 position of **11c** was shifted to R_3 position, which we expected to make the distance from the amide moiety of **11c** to Ser111 and Asn114 closer, while making that of **11c** to Tyr106 further. To evaluate our design of compound **12**, we superimposed the crystal structure of FLT3 (PDB code:1RJB)[28] to that of TAK1 (Figure 5 (C) right) and found a critical difference between the structure of TAK1 and FLT3; namely, that near the amide carbonyl group of **12** at R_3 position, Ser111 was located in TAK1, but Asp698 in FLT3. With TAK1, the amide carbonyl interacted with Ser111, whereas in FLT3, this amide carbonyl had repulsive coulomb against Asp698. We supposed this difference could give **12** TAK1 selectivity against FLT3.

As expected, **12** showed an excellent kinase selectivity profile in both in-house and KinomeScan™ panel assays and possessed potent TAK1 inhibitory activity (IC_{50}=11 nM). In the in-house panel data of 38 kinases, we could not see potent inhibitory activity (IC_{50} > 10 μM) except against TAK1. Particularly, the IC_{50} of FLT3 was 35000 nM, which indicated that compound **12** had about 3200 times more potent inhibitory activity on TAK1 than on FLT3. In the 442-kinase panel data, **12** showed inhibition against only 3 kinases other than TAK1 at 1.0 μM. The other 3 kinases are MAP4K4, PIP5K1C, and PIP5K2C. MAP4K4 is an upstream kinase of TAK1, and the other two kinases are lipid kinases. To find out why **12** had a high TAK1 selectivity profile, the X-ray structure of TAK1 and **12** complex was solved (Figure 5 (C) left). The binding mode of **11c** and **12** was very similar basically, but three differences existed that would afford the high TAK1 selectivity profile of **12**. The first one was acquiring the interaction with Ser111 and Asn114, which was a rare and unique combination of amino acid residues in TAK1. As expected, the distances from the carbonyl group at R_3 position of **12** to Ser 111 and Asn114 were 3.4 Å and 4.2 Å, respectively, which is closer than those in **11c**. The second one was that compound **12** had repulsive coulomb interactions against kinases with Asp or Glu corresponding to Ser111 in TAK1. From our analysis, 252 out of 490 kinases had Asp or Glu corresponding to Ser111 in TAK1, and these kinases were considered to possess a repulsive coulomb interaction against compound **12**, which resulted in TAK1 selectivity. The third one was reducing the interaction between the inhibitor and

Tyr106 in TAK1 at the hinge region. The distance from the benzene ring of **12** to Tyr106 in TAK1 is 4.2 Å. In contrast, the distance form N-methyl piperazine ring of **11c** to Tyr106 is 3.4 Å. 304/490 kinases have an aromatic residue corresponding to Tyr106 in TAK1. Decreasing this interaction reduced the activity of the above-mentioned 304 kinases, including TAK1. Even though TAK1 inhibitory activity was also decreased, we considered that TAK1 selectivity was improved. According to these factors, we were able to discover compound **12** which was a potent TAK1 inhibitor with excellent selectivity.

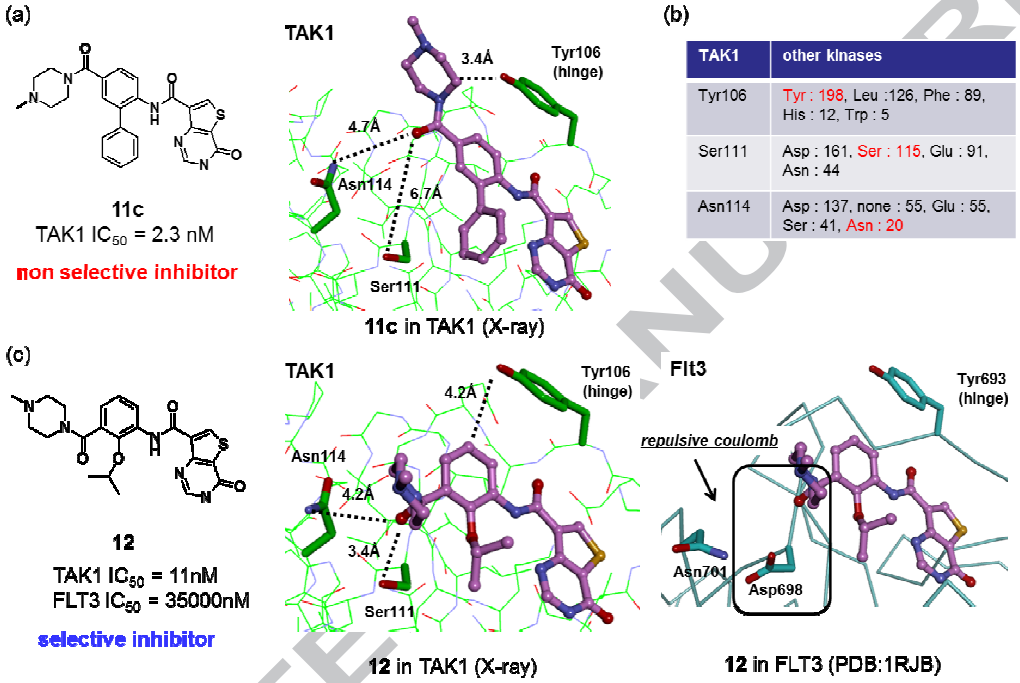

Figure 5. (a) X-ray crystal structure of **11c** in TAK1(PDB code:5JGA). Compound **11c** is shown as a ball and stick model colored by element type (C in magenta, O in red, N in blue, S in yellow). Amino acid residues of TAK1 that interact with compound **11c** are shown in the same colors except for C in light green. The key hydrogen bonding interactions are depicted as dotted lines (b) Amino acid residues corresponding to Tyr106, Ser 111, and Asn114 of TAK1 in a 490 kinase in-house database. (c) **12** in the crystal structure of TAK1 (left, PDB code:5JGD) and in that FLT3 (right). Compound **12** is shown as a ball and stick model colored by element type (C in magenta, O in red, N in blue, S in yellow). Amino acid residues of TAK1 and FLT3 that interact with compound **12** are shown in the same colors except for C, which is light green in TAK1 and cyan in FLT3. The key hydrogen bonding interactions are depicted as dotted lines.

4. Conclusion

In summary, we have discovered a potent inhibitor that is highly selective to TAK1 by using the SBDD approach to develop a novel series of thienopyrimidinones. After hit compound **8** was obtained by a

chemogenomics approach, it was modified to give **9b** with increased TAK1 inhibitory activity and solubility, but its metabolic stability was low. Metabolites identified from **9b** included **10** with potent TAK1 inhibition. X-ray information revealed that the carboxyl group in thienopyrimidinone played a key role in acquiring the potent TAK1 inhibitory activity. Next, we were able to obtain a more potent TAK1 inhibitor **11c** (IC_{50}=2.3 nM) by adjusting the volume of R_2 group, but TAK1 selectivity was low. To improve this kinase selectivity, we conducted two strategies utilizing 3D structure information: one targeting unique amino acid residues in TAK1, especially the combination of Ser111 and Asn114; the other decreasing the interaction between the amide moiety at R_4 group in the solvent region and Tyr106 at the hinge position in TAK1, which has an aromatic side chain that is highly conserved between protein kinases. As expected, **12** showed an excellent TAK1 selectivity profile in both an in-house and a KinomeScan™ panel assay and possessed potent TAK1 inhibitory activity (IC_{50}=11 nM). Particularly, the in-house 38-kinase panel data did not reveal potent inhibitory activity (IC_{50} < 10 μM) of kinases other than TAK1.

We could obtain the potent and highly selective TAK1 inhibitor **12**, but cell activity was weak (IC_{50} > 5 μM, SW982 cells :TNF-α-induced IL-6 production) because of low permeability (Caco-2 Papp < $1.0x10^{-6}$ cm/sec). So, further optimization of this series to improve permeability and other physicochemical property is ongoing.

5. Experimental

5.1. Chemistry: general

Purchased reagents and solvents were used without further purification unless otherwise noted. ^{1}H and ^{13}C spectra were recorded on VARIAN 400-MR or Bruker AVANCE 2 or 3 and chemical shifts are expressed in parts per million (ppm) from trimethylsilane (TMS) as an internal standard. The spectrum patterns are described as follows: s = singlet, d = doublet, t = triplet, q = quartet, br = broad, m = multiplet. LC-MS were measured by a Waters ACQUITY SQD electrospray ionization (ESI) system. High resolution mass spectra (HRMS) were measured with a Waters I-Class/Xevo G2S TOF MS spectrometer using an ESI source coupled to a Waters HPLC system operating in reversed phase with an Ascentis Express C18 (2.7 μm, 2.1 mm x 50 mm) column or no column. Flash column chromatography was performed with Purif-pack® or Biotage SNAP® cartridges. NH-silica gel chromatography and preparative TLC were conducted with FUJI SILYSIA NH-DM1020 and Merck silica gel 60 PF_{254}, respectively. Reversed column chromatography was conducted with an ODS column, Wakosil® 25C18.

5.1.1. 4-Chloro-7-methylthieno[3,2-d]pyrimidine (14)

Commercially available methyl 3-amino-4-methylthiophene-2-carboxylate **13** (16.5 g, 96.0 mmol) was dissolved in formamide (100 mL) and stirred at 150 °C under nitrogen atmosphere. After the starting material consumption had been confirmed by LC-MS, the reaction mixture was cooled to room temperature and then

H_2O (500 mL) was added to the mixture. The suspension was filtered to collect a white solid that was dried by an oil pump to give 7-methylthieno[3,2-d]pyrimidin-4(3H)-one (12.2 g). The solid was used for the next reaction without further purification.

The aforementioned 7-methylthieno[3,2-d]pyrimidin-4(3H)-one (1.85 g) was treated with $POCl_3$ (8.80 mL) and stirred at 100 °C for 6h. The reaction mixture was cooled to 0 °C, poured into ice-water/ethyl acetate, and extracted with ethyl acetate twice. The organic layer was washed with brine, dried over Na_2SO_4, and filtered. The organic solvent was concentrated under reduced pressure to give a crude residue. Water (200 mL) was added to the residue and the mixture cooled at 5 °C in the refrigerator for a day. The suspension was filtered to afford **14** (1.90 g, 2steps 72%) as a white solid. ^{1}H-NMR (400 MHz, DMSO-D_6) δ: 9.07 (1H, s), 8.25 (1H, d, *J* = 1.2 Hz), 2.45 (3H, d, *J* = 1.2 Hz). ^{13}C-NMR (100 MHz, DMSO-D_6) δ: 160.7, 153.9, 153.6, 133.9, 133.2, 130.0, 12.5. HRMS (ESI-TOF) m/z: $[M+H]^+$ Calcd for $C_7H_6ClN_2S$ 184.9940; Found 184.9937.

5.1.2. 7-Methylthieno[3,2-d]pyrimidine (15)

A solution of ethyl acetate/2-propanol = 5/1 (v/v, 200 mL) was added to $Pd(OH)_2$ (4.83 g, 20% on carbon, wetted with ca.50% water) under nitrogen atmosphere and filled with hydrogen. A solution of **14** (9.65 g, 51.7 mmol) in ethyl acetate/2-propanol = 5/1 (v/v, 50.0 mL) and Et_3N (16.6 mL, 119 mmol) was added to the suspension and filled with hydrogen again. The suspension was stirred at room temperature for 20 h. The reaction mixture was filtered with Celite® and concentrated. After the addition of ethyl acetate and saturated $NaHCO_3$ aq. to the residue, the ethyl acetate extraction was executed twice. The combined organic layer was washed with brine, dried over Na_2SO_4, and filtered. The organic solution was concentrated under reduced pressure to afford **15** (7.30 g, 94%). ^{1}H-NMR (400 MHz, DMSO-D_6) δ: 9.50 (1H, s), 9.19 (1H, s), 8.15 (1H, d, *J* = 1.2 Hz), 2.44 (3H, d, *J* = 1.2 Hz). ^{13}C-NMR (100 MHz, DMSO-D_6) δ: 159.0, 153.8, 152.4, 133.1, 132.0, 131.3, 12.1. HRMS (ESI-TOF) m/z: $[M+H]^+$ Calcd for $C_7H_7N_2S$ 151.0330; Found 151.0332.

5.1.3. Thieno[3,2-d]pyrimidine-7-carboxylic acid (16)

A solution of **15** (1.00 g, 6.66 mmol), NBS (2.97 g, 16.7 mmol) and benzoyl peroxide (322 mg, 1.33 mmol) in CCl_4 (67.0 mL) was stirred at reflux for 2.5 h. The reaction mixture was cooled to room temperature and filtered. The organic solvent was evaporated to give 7-(dibromomethyl)thieno[3,2-d]pyrimidine as a crude residue. The residue was used for the next reaction without further purification.

To the aforementioned residue was added H_2O (40.0 mL) and pyridine (4.00 mL) and the mixture was stirred at 100 °C for 1.5 h. The reaction mixture was diluted with ethyl acetate and extracted. The organic layer was washed with brine, dried over Na_2SO_4 and concentrated. The obtained white solid was washed with hexane/ethyl acetate = 4/1 (v/v) to afford thieno[3,2-d]pyrimidine-7-carbaldehyde (796 mg) as a crude residue. The residue was used for the next reaction without further purification.

To a solution of the aforementioned residue (796 mg) in acetone/H_2O = 2/1 (v/v, 99.0 mL) was added $NaClO_2$ (658 mg, 7.28 mmol) and sulfamic acid (1.17 g, 12.1 mmol) at 0 °C and then stirred at 40 °C for 2 h.

The reaction mixture was evaporated to give a white solid. The solid was washed with H_2O and ethyl acetate to afford **16** (690 mg, 3 steps 58%). ^{1}H-NMR (400 MHz, DMSO-D_6) δ: 12.98 (1H, br s), 9.63 (1H, s), 9.28 (1H, s), 9.18 (1H, s). ^{13}C-NMR (100 MHz, DMSO-D_6) δ: 162.0, 156.8, 154.6, 153.4, 147.0, 132.0, 127.3. HRMS (ESI-TOF) m/z: $[M+H]^+$ Calcd for $C_7H_5N_2O_2S$ 181.0071; Found 181.0069.

5.1.4. 4-Chloro-7-(dibromomethyl)thieno[3,2-d]pyrimidine (17)

To a solution of **14** (4.00 g, 21.4 mmol) in CCl_4 (43.0 mL) was added NBS (9.50 g, 53.5 mmol) and AIBN (703 mg, 4.28 mmol) at room temperature. The reaction mixture was stirred at reflux for 4 h under nitrogen atmosphere. After the reaction mixture was filtered and evaporated, the obtained residue was purified by flash column chromatography (hexane/ethyl acetate) to afford **17** (6.92 g) as a semi-pure product. The residue was used for the next reaction without further purification.

5.1.5. 4-Oxo-3,4-dihydrothieno[3,2-d]pyrimidine-7-carbaldehyde (18)

The above semi-pure **17** (6.92 g) was treated with methanol (200 mL) and stirred at 70 °C for 24 h to generate 7-(dimethoxymethyl)-4-methoxythieno[3,2-d]pyrimidine. The reaction mixture was evaporated and the residue was diluted with THF (100 mL). To the solution was added 5N HCl aq. (100 mL) and the mixture was stirred at 60 °C for 3 h. After the reaction mixture was evaporated, the obtained solid was collected by filtration and dried under reduced pressure to afford **18** as a crude product. The crude product was used for the next reaction without further purification.

5.1.6. 4-Oxo-3,4-dihydro-thieno[3,2-d]pyrimidine-7-carboxylic acid (19)

To a solution of the above crude product **18** in acetone (200 mL) and H_2O (100 mL) was added $NaClO_2$ (2.90 g, 32.1 mmol) and sulfamic acid (5.20 g, 53.5 mmol). The reaction mixture was stirred at room temperature for 2 h. After the reaction mixture was evaporated, the obtained solid was washed with H_2O and acetone and dried under reduced pressure to afford **19** (2.96 g, 3 steps 71%) as a white solid. ^{1}H-NMR (400 MHz, DMSO-D_6) δ: 12.90-12.79 (2H, br m), 8.85 (1H, s), 8.27 (1H, s). ^{13}C-NMR (100 MHz, DMSO-D_6) δ: 162.1, 157.3, 154.6, 147.5, 142.3, 128.5, 124.4. HRMS (ESI-TOF) m/z: $[M-H]^-$ Calcd for $C_7H_3N_2O_3S$ 194.9865; Found 194.9865.

5.1.7. N-(2-methoxy-4-((3-(4-methylpiperazin-1-yl)propyl)carbamoyl)phenyl)thieno[3,2-d]pyrimidine-7-carboxamide (9b)

To a solution of 4-amino-3-methoxy-N-(3-(4-methylpiperazin-1-yl)propyl)benzamide **20b** (52.0 mg, 0.170 mmol) and thieno[3,2-d]pyrimidine-7-carboxylic acid **16** (31.0 mg, 0.170 mmol) in acetonitrile (3.50 mL) was added HATU (129 mg, 0.340 mmol) and DIPEA (59.0 μL, 0.340 mmol) and stirred at 80 °C. After confirming the starting material consumption by LC-MS, the reaction mixture was concentrated to give a crude residue. The crude residue was purified by column chromatography utilizing NH silica gel (DCM/methanol) to afford

9b (54.0 mg, 68%) as a yellow solid. ^{1}H-NMR (400 MHz, $CDCl_3$) δ: 11.91 (1H, s), 9.40 (1H, s), 9.38 (1H, s), 9.05 (1H, s), 8.69 (1H, d, *J* = 8.8 Hz), 8.29 (1H, t, *J* = 4.6 Hz), 7.64 (1H, d, *J* = 1.5 Hz), 7.39 (1H, dd, *J* = 8.3, 1.5 Hz), 4.11 (3H, s), 3.60-3.59 (2H, m), 2.75-2.63 (10H, m), 2.33 (3H, s), 1.82-1.80 (2H, m). ^{13}C-NMR (100 MHz, DMSO-D_6) δ: 165.4, 158.4, 155.2, 154.3, 153.9, 148.1, 146.7, 132.5, 130.2, 130.0, 128.5, 119.9, 118.5, 109.8, 56.3, 55.7, 54.8, 52.7, 45.8, 38.0, 26.3. HRMS (ESI-TOF) m/z: $[M+H]^+$ Calcd for $C_{23}H_{29}N_6O_3S$ 469.2022; Found 469.2027.

5.1.8. N-(2-methoxy-4-(4-methylpiperazine-1-carbonyl)phenyl)thieno[3,2-d]pyrimidine-7-carboxamide (9a)

Compound **9a** was synthesized by a similar procedure to **9b**. The yield was 36%. Yellow solid. ^{1}H-NMR (400 MHz, $CDCl_3$) δ: 11.83 (1H, s), 9.40 (1H, s), 9.38 (1H, s), 9.05 (1H, s), 8.63 (1H, d, *J* = 7.8 Hz), 7.11 (1H, d, *J* = 2.0 Hz), 7.06 (1H, dd, *J* = 8.3, 1.5 Hz), 4.06 (3H, s), 3.73-3.71 (4H, m), 2.44 (4H, br s), 2.34 (3H, s). ^{13}C-NMR (100 MHz, DMSO-D_6) δ: 168.6, 158.3, 155.2, 154.3, 153.9, 148.3, 146.7, 132.5, 131.3, 128.8, 128.5, 119.6, 118.9, 110.0, 56.4, 45.6. HRMS (ESI-TOF) m/z: $[M+H]^+$ Calcd for $C_{20}H_{22}N_5O_3S$ 412.1443; Found 412.1444.

5.1.9 N-(2-methoxy-4-(4-methylpiperazin-1-yl)phenyl)thieno[3,2-d]pyrimidine-7-carboxamide (9c)

Compound **9c** was synthesized by a similar procedure to **9b**. The yield was 57%. Yellow solid. ^{1}H-NMR (400 MHz, $CDCl_3$) δ: 11.53 (1H, s), 9.38 (1H, s), 9.35 (1H, s), 9.00 (1H, s), 8.44 (1H, dd, *J* = 6.1, 3.1 Hz), 6.58 (2H, dd, *J* = 6.7, 2.4 Hz), 4.01 (3H, s), 3.23 (4H, t, *J* = 5.2 Hz), 2.61 (4H, t, *J* = 4.9 Hz), 2.37 (3H, s). ^{13}C-NMR (100 MHz, DMSO-D_6) δ: 157.5, 155.2, 154.2, 153.8, 149.6, 148.3, 145.6, 132.5. 129.1, 120.4, 119.7, 106.7, 99.8, 56.1, 54.6, 48.4, 45.8. HRMS (ESI-TOF) m/z: $[M+H]^+$ Calcd for $C_{19}H_{22}N_5O_2S$ 384.1494; Found 384.1501.

5.1.10. 4-amino-3-methoxy-N-(3-(4-methylpiperazin-1-yl)propyl)benzamide (20b)

To a solution of commercially available 3-methoxy-4-nitrobenzoic acid **21** (100 mg, 0.507 mmol) and 3-(4-methylpiperazin-1-yl)propan-1-amine (159 mg, 1.01 mmol) in DCM (5.00 mL) was added HATU (386 mg, 1.01 mmol) at room temperature and stirred at the same temperature. After confirming the starting material consumption by LC-MS, the reaction mixture was concentrated to give a crude residue. The crude residue was purified by column chromatography utilizing NH silica gel (DCM/methanol) to afford 3-methoxy-N-(3-(4-methylpiperazin-1-yl)propyl)-4-nitrobenzamide (quant).

Ethanol (3.50 mL) was added to 10% Pd/C (76.0 mg) under nitrogen atmosphere and filled with hydrogen. A solution of 3-methoxy-N-(3-(4-methylpiperazin-1-yl)propyl)-4-nitrobenzamide (151 mg, 0.449 mmol) in ethanol (1.00 mL) was added to the suspension, filled with hydrogen again and then stirred at 40 °C. After the starting material consumption had been confirmed by LC-MS, the reaction mixture was filtered with Celite® and concentrated. The obtained residue was purified by column chromatography utilizing NH silica gel

(DCM/methanol) to afford **20b** (118 mg, 86%) as a light yellow oil. ^{1}H-NMR (400 MHz, CD_3OD) δ: 7.33 (1H, d, *J* = 1.5 Hz), 7.28 (1H, dd, *J* = 8.3, 2.0 Hz), 6.70 (1H, d, *J* = 8.3 Hz), 3.89 (3H, s), 3.39 (2H, t, *J* = 6.8 Hz), 3.00-2.28 (10H, m), 2.27 (3H, s), 1.83-1.77 (2H, m). ^{13}C-NMR (100 MHz, CD_3OD) δ: 170.4, 147.9, 142.4, 123.9, 122.1, 114.3, 110.5, 57.3, 56.1, 55.6, 53.7, 45.9, 39.4, 27.4. HRMS (ESI-TOF) m/z: $[M+H]^+$ Calcd for $C_{16}H_{27}N_4O_2$ 307.2134; Found 307.2146.

5.1.11. (4-amino-3-methoxyphenyl)(4-methylpiperazin-1-yl)methanone (20a)

Compound **20a** was synthesized by a similar procedure to **20b**. The yield was 80% (2 steps). Light yellow oil. ^{1}H-NMR (400 MHz, $CDCl_3$) δ: 6.94 (1H, d, *J* = 1.5 Hz), 6.86 (1H, dd, *J* = 8.1, 1.7 Hz), 6.65 (1H, d, *J* = 8.3 Hz), 3.99 (2H, br s), 3.87 (3H, s), 3.66 (4H, br s), 2.41 (4H, br s), 2.32 (3H, s). ^{13}C-NMR (100 MHz, $CDCl_3$) δ: 171.1, 146.8, 138.5, 124.4, 121.0, 113.4, 110.3, 55.6, 54.6, 45.4. HRMS (ESI-TOF) m/z: $[M+H]^+$ Calcd for $C_{13}H_{20}N_3O_2$ 250.1555; Found 250.1560.

5.1.12. 2-methoxy-4-(4-methylpiperazin-1-yl)aniline (20c)

A solution of commercially available 4-fluoro-2-methoxy-1-nitrobenzene (**22)** (200 mg, 1.17 mmol), N-methyl piperazine (154 µL, 1.40 mmol) and Et_3N (329 µL, 2.34 mmol) in DMA (2.00 mL) was stirred at 150 °C for 15 min utilizing a microwave reactor. The solution was purified by column chromatography utilizing NH silica gel (DCM/Methanol) to afford 1-(3-methoxy-4-nitrophenyl)-4-methylpiperazine (282 mg, 96%).

To a solution of 1-(3-methoxy-4-nitrophenyl)-4-methylpiperazine (200 mg, 0.796 mmol) in methanol (5.00 mL) was added 10% Pd/C (50.0 mg) under nitrogen atmosphere and then filled with hydrogen (3 times). The suspension was stirred at room temperature for 2 h. After the starting material consumption had been confirmed by LC-MS, the reaction mixture was filtered with Celite® and concentrated. The obtained residue was purified by column chromatography utilizing NH silica gel (DCM/methanol) to afford **20c** (147 mg, 84%) as a dark brown oil. ^{1}H-NMR (400 MHz, DMSO-D_6) δ: 6.51-6.48 (2H, m), 6.27 (1H, dd, *J* = 8.4, 2.6 Hz), 4.19 (2H, s), 3.73 (3H, s), 2.94-2.93 (4H, m), 2.43-2.42 (4H, m), 2.20 (3H, s). ^{13}C-NMR (100 MHz, DMSO-D_6) δ: 147.0, 143.3, 130.9, 114.2, 108.5, 101.8, 55.2, 54.9, 50.2, 45.8. HRMS (ESI-TOF) m/z: $[M+H]^+$ Calcd for $C_{12}H_{20}N_3O$ 222.1606; Found 222.1618.

5.1.13. N-(2-methoxy-4-((3-(4-methylpiperazin-1-yl)propyl)carbamoyl)phenyl)-4-oxo-3,4-dihydrothieno [3,2-d]pyrimidine-7-carboxamide (10)

To a solution of 4-oxo-3,4-dihydro-thieno[3,2-d]pyrimidine-7-carboxylic acid **(19)** (15.0 mg, 0.0760 mmol) and 4-amino-3-methoxy-N-(3-(4-methylpiperazin-1-yl)propyl)benzamide **(20b)** (23.0 mg, 0.0760 mmol) in acetonitrile (1.50 mL) was added HATU (29.0 mg, 0.152 mmol) and DIPEA (26.0 µL, 0.152 mmol) and stirred at 80 °C. After the starting material consumption had been confirmed by LC-MS, the reaction mixture was concentrated to give a crude residue. The obtained residue was purified by column chromatography utilizing

NH silica gel (DCM/methanol) to afford **10** (24.0 mg, 65%) as a light yellow solid. ^{1}H-NMR (400 MHz, DMSO-D_6) δ: 12.94 (1H, s), 11.94 (1H, s), 8.92 (1H, s), 8.54-8.53 (2H, m), 8.45-8.44 (1H, m), 7.54 (1H, d, J = 1.5 Hz), 7.50 (1H, dd, J = 8.3, 2.0 Hz), 4.03 (3H, s), 3.28-3.26 (4H, br m), 2.42-2.35 (8H, br m), 2.15 (3H, s), 1.71-1.64 (2H, m). ^{13}C-NMR (100 MHz, DMSO-D_6) δ: 165.4, 158.7, 157.9, 152.9, 148.7, 148.2, 141.0, 130.3, 130.1, 129.8, 124.3, 119.8, 118.4, 109.7, 56.2, 55.7, 54.7, 52.7, 45.7, 37.9, 26.3. HRMS (ESI-TOF) m/z: $[M+H]^+$ Calcd for $C_{23}H_{29}N_6O_4S$ 485.1971; Found 485.1995.

Compounds **11a**-**11l** and **12** were synthesized by a similar procedure to **10**.

5.1.14. N-(2-methyl-4-(4-methylpiperazine-1-carbonyl)phenyl)-4-oxo-3,4-dihydrothieno[3,2-d]pyrimidine -7-carboxamide (11a)

The yield was 28%. White solid. ^{1}H-NMR (600 MHz, TFA-D) δ: 9.33 (1H, s), 9.28 (1H, s), 7.55 (1H, d, *J* = 8.2 Hz), 7.48 (1H, s), 7.42 (1H, d, *J* = 8.0 Hz), 5.02 (1H, d, *J* = 14.3 Hz), 4.15 (1H, d, *J* = 14.6 Hz), 3.84-3.83 (2H, m), 3.70-3.68 (1H, m), 3.57-3.54 (1H, m), 3.36-3.34 (1H, m), 3.25-3.22 (1H, m), 3.10 (3H, s), 2.37 (3H, s). ^{13}C-NMR (150 MHz, TFA-D) δ: 175.3, 163.4, 157.8, 151.3, 145.6, 145.5, 138.7, 137.9, 133.9, 132.2, 129.5, 127.9, 127.8, 125.7, 56.2, 47.0, 45.7, 42.1, 18.3. HRMS (ESI-TOF) m/z: $[M+H]^+$ Calcd for $C_{20}H_{22}N_5O_3S$ 412.1443; Found 412.1444.

5.1.15. N-(2-isopropyl-4-(4-methylpiperazine-1-carbonyl)phenyl)-4-oxo-3,4-dihydrothieno [3,2-d]pyrimidine-7-carboxamide (11b)

The yield was 56%. White solid. ^{1}H-NMR (400 MHz, DMSO-D_6) δ: 12.99 (1H, br s), 11.47 (1H, s), 8.91 (1H, s), 8.48 (1H, s), 8.26 (1H, d, *J* = 8.2 Hz), 7.36 (1H, d, *J* = 2.0 Hz), 7.27 (1H, dd, *J* = 8.4, 2.0 Hz), 3.40-3.36 (5H, m), 2.34-2.31 (4H, m), 2.20 (3H, s), 1.31 (3H, s), 1.30 (3H, s). ^{13}C-NMR (100 MHz, DMSO-D_6) δ: 168.9, 158.9, 158.2, 152.8, 148.9, 140.8, 138.3, 136.2, 131.6, 130.0, 125.1, 124.5, 124.3, 121.6, 54.5, 45.6, 27.5, 22.6. HRMS (ESI-TOF) m/z: $[M+H]^+$ Calcd for $C_{22}H_{26}N_5O_3S$ 4401756; Found 440.1758.

5.1.16. N-(5-(4-methylpiperazine-1-carbonyl)-[1,1'-biphenyl]-2-yl)-4-oxo-3,4-dihydrothieno [3,2-d]pyrimidine-7-carboxamide (11c)

The yield was 97%. Light yellow solid. ^{1}H-NMR (400 MHz, DMSO-D_6) δ: 11.26 (1H, s), 8.86 (1H, s), 8.60 (1H, d, *J* = 8.3 Hz), 7.57-7.46 (7H, m), 7.26 (1H, d, *J* = 2.2 Hz), 3.52 (4H, br s), 2.32 (4H, br s), 2.19 (3H, s). ^{13}C-NMR (100 MHz, DMSO-D_6) δ: 168.4, 158.9, 158.7, 152.5, 148.1, 140.7, 137.4, 136.9, 132.5, 131.0, 129.7, 129.6, 129.0, 128.9, 127.9, 127.1, 123.9, 120.7, 54.6, 45.6. HRMS (ESI-TOF) m/z: $[M-H]^-$ Calcd for $C_{25}H_{22}N_5O_3S$ 472.1443; Found 472.1450.

5.1.17. N-(2-cyclohexyl-4-(4-methylpiperazine-1-carbonyl)phenyl)-4-oxo-3,4-dihydrothieno [3,2-d]pyrimidine-7-carboxamide (11d)

The yield was 46%. White solid. ^{1}H-NMR (400 MHz, DMSO-D_6) δ: 13.02 (1H, s), 11.21 (1H, s), 8.97 (1H,

s), 8.42 (1H, s), 8.20 (1H, d, *J* = 8.4 Hz), 7.34 (1H, d, *J* = 1.8 Hz), 7.27 (1H, dd, *J* = 8.4, 2.0 Hz), 3.58-3.41 (4H, m), 2.33 (4H, br s), 2.20 (3H, s), 1.86-1.83 (5H, m), 1.75-1.72 (1H, m), 1.47-1.44 (4H, m), 1.29-1.23 (1H, m). ^{13}C-NMR (100 MHz, DMSO-D_6) δ: 168.9, 158.7, 157.3, 152.7, 148.0, 141.4, 137.5, 135.9, 131.8, 130.1, 125.0, 124.5, 122.1, 54.5, 45.6, 37.7, 32.8, 26.5, 25.6. HRMS (ESI-TOF) m/z: $[M+H]^+$ Calcd for $C_{25}H_{30}N_5O_3S$ 480.2069; Found 480.2068.

5.1.18. N-(2-fluoro-4-(4-methylpiperazine-1-carbonyl)phenyl)-4-oxo-3,4-dihydrothieno [3,2-d]pyrimidine-7-carboxamide (11e)

The yield was 78%. White solid. ^{1}H-NMR (600 MHz, TFA-D) δ: 9.34 (1H, s), 9.29 (1H, s), 8.01 (1H, dd, *J* = 7.8, 7.8 Hz), 7.42-7.41 (2H, m), 5.02 (1H, d, *J* = 13.4 Hz), 4.18-4.15 (1H, m), 3.86-3.85 (2H, m), 3.74-3.73 (1H, m), 3.58-3.55 (1H, m), 3.36-3.28 (2H, m), 3.12 (3H, s). ^{13}C-NMR (150 MHz, TFA-D) δ: 173.7, 163.2, 158.1, 157.9, 156.4, 151.2, 145.8, 145.7, 133.7, 128.4, 128.0, 127.7, 126.0, 125.9, 56.1, 47.0, 45.7, 42.1. HRMS (ESI-TOF) m/z: $[M+H]^+$ Calcd for $C_{19}H_{19}FN_5O_3S$ 416.1193; Found 416.1187.

5.1.19. N-(2-chloro-4-(4-methylpiperazine-1-carbonyl)phenyl)-4-oxo-3,4-dihydrothieno [3,2-d]pyrimidine-7-carboxamide (11f)

The yield was 75%. White solid. ^{1}H-NMR (600 MHz, TFA-D) δ: 9.36 (1H, s), 9.26 (1H, s), 8.03 (1H, br s), 7.71 (1H, s), 7.53 (1H, br s), 5.02-5.00 (1H, m), 4.14-4.12 (1H, m), 3.93-3.86 (2H, m), 3.75-3.73 (1H, m), 3.62-3.61 (1H, m), 3.34-3.26 (2H, m), 3.10 (3H, s). ^{13}C-NMR (150 MHz, TFA-D) δ: 173.7, 163.2, 157.9, 151.4, 145.9, 145.4, 137.1, 133.9, 131.5, 131.3, 128.8, 128.4, 127.8, 126.1, 55.9, 47.1, 45.7, 42.2. HRMS (ESI-TOF) m/z: $[M+H]^+$ Calcd for $C_{19}H_{19}ClN_5O_3S$ 432.0897; Found 432.0897.

5.1.20. N-(2-bromo-4-(4-methylpiperazine-1-carbonyl)phenyl)-4-oxo-3,4-dihydrothieno [3,2-d]pyrimidine-7-carboxamide (11g)

The yield was 40%. White solid. ^{1}H-NMR (600 MHz, TFA-D) δ: 9.34 (1H, s), 9.24 (1H, s), 7.99 (1H, d, *J* = 8.3 Hz), 7.86 (1H, s), 7.56 (1H, d, *J* = 8.4 Hz), 5.02-4.99 (1H, m), 4.15-4.13 (1H, m), 3.88-3.85 (2H, m), 3.73-3.71 (1H, m), 3.57-3.55 (1H, m), 3.36-3.27 (2H, m), 3.11 (3H, s). ^{13}C-NMR (150 MHz, TFA-D) δ: 173.5, 163.2, 157.9, 151.3, 145.8, 145.3, 138.5, 134.4, 134.1, 129.4, 128.5, 127.8, 126.1, 121.0, 56.0, 47.0, 45.7, 42.2. HRMS (ESI-TOF) m/z: $[M+H]^+$ Calcd for $C_{19}H_{19}BrN_5O_3S$ 476.0392; Found 476.0396.

5.1.21. N-(2-methoxy-4-(4-methylpiperazine-1-carbonyl)phenyl)-4-oxo-3,4-dihydrothieno [3,2-d]pyrimidine-7-carboxamide (11h)

The yield was 97%. White solid. ^{1}H-NMR (400 MHz, DMSO-D_6) δ: 12.53 (1H, br s), 11.56 (1H, s), 8.85 (1H, s), 8.49 (1H, d, *J* = 8.1 Hz), 8.37 (1H, s), 7.14 (1H, s), 7.08 (1H, d, *J* = 8.6 Hz), 4.00 (3H, s), 3.71 (4H, br s), 3.18 (4H, br s), 2.79 (3H, s). ^{13}C-NMR (100 MHz, DMSO-D_6) δ: 169.3, 159.1, 157.5, 153.3, 148.8, 148.4, 142.0, 130.6, 130.2, 129.9, 124.9, 120.4, 119.3, 110.6, 56.8, 52.9, 46.0, 43.0. HRMS (ESI-TOF) m/z: $[M+H]^+$

Calcd for $C_{20}H_{22}N_5O_4S$ 428.1393; Found 428.1400.

5.1.22. N-(2-isopropoxy-4-(4-methylpiperazine-1-carbonyl)phenyl)-4-oxo-3,4-dihydrothieno [3,2-d]pyrimidine-7-carboxamide (11i)

The yield was 93%. White solid. ^{1}H-NMR (400 MHz, DMSO-D_6) δ: 12.99 (1H, br s), 11.68 (1H, s), 8.94 (1H, s), 8.55 (1H, d, *J* = 8.4 Hz), 8.33 (1H, s), 7.11 (1H, d, *J* = 1.6 Hz), 6.99 (1H, dd, *J* = 8.4, 1.6 Hz), 4.84-4.74 (1H, m), 3.50 (4H, br s), 2.32 (4H, br s), 2.20 (3H, s), 1.40 (3H, s), 1.39 (3H, s). ^{13}C-NMR (100 MHz, DMSO-D_6) δ: 168.6, 158.5, 157.3, 152.7, 147.6, 146.1, 141.4, 131.2, 130.3, 129.8, 124.5, 119.4, 119.3, 112.1, 71.0, 54.5, 45.6, 21.9. HRMS (ESI-TOF) m/z: $[M+H]^+$ Calcd for $C_{22}H_{26}N_5O_4S$ 456.1705; Found 456.1709.

5.1.23. N-(2-((1,1,1,3,3,3-hexafluoropropan-2-yl)oxy)-4-(4-methylpiperazine-1-carbonyl)phenyl)-4-oxo-3,4-dihydrothieno[3,2-d]pyrimidine-7-carboxamide (11j)

The yield was 21%. White solid. ^{1}H-NMR (DMSO-D_6) δ: 12.91 (1H, br s), 11.69 (1H, s), 9.00 (1H, s), 8.66 (1H, d, *J* = 8.3 Hz), 8.04 (1H, s), 7.62 (1H, s), 7.31 (1H, dd, *J* = 8.4, 1.6 Hz), 6.86-6.80 (1H, m), 3.63 (4H, br s), 3.03 (4H, br s), 2.69 (3H, s). ^{13}C-NMR (100 MHz, DMSO-D_6) δ: 167.9, 158.8, 156.8, 152.5, 146.9, 144.8, 142.2, 130.2, 129.6, 129.5, 128.8, 124.6, 123.2, 122.6, 120.6, 119.8, 112.8, 52.8, 43.0. HRMS (ESI-TOF) m/z: $[M+H]^+$ calcd for $C_{22}H_{20}F_6N_5O_4S$ 564.1140; Found 564.1141.

5.1.24. N-(2-(dimethylamino)-4-(4-methylpiperazine-1-carbonyl)phenyl)-4-oxo-3,4-dihydrothieno [3,2-d]pyrimidine-7-carboxamide (11k)

The yield was 92%. White solid. ^{1}H-NMR (DMSO-D_6) δ: 12.01 (1H, s), 8.89 (1H, d, *J* = 1.6 Hz), 8.54 (1H, d, *J* = 8.4 Hz), 8.50 (1H, s), 7.23 (1H, d, *J* = 1.8 Hz), 7.13 (1H, dd, *J* = 8.3, 1.9 Hz), 3.51 (4H, br s), 2.73 (6H, s), 2.33 (4H, br s), 2.20 (3H, s). ^{13}C-NMR (100 MHz, DMSO-D_6) δ: 168.7, 158.6, 157.2, 152.9, 147.8, 143.5, 141.4, 134.4, 130.9, 130.5, 124.3, 122.8, 119.1, 54.5, 45.6, 44.0. HRMS (ESI-TOF) m/z: $[M+H]^+$ Calcd for $C_{21}H_{25}N_6O_3S$ 441.1709; Found 441.1726.

5.1.25. N-(2-(ethyl(methyl)amino)-4-(4-methylpiperazine-1-carbonyl)phenyl)-4-oxo-3,4-dihydrothieno [3,2-d]pyrimidine-7-carboxamide (11l)

The yield was 47%. White solid. ^{1}H-NMR (400 MHz, DMSO-D_6) δ: 12.47 (1H, br s), 11.72 (1H, s), 8.85 (1H, s), 8.53 (1H, d, *J* = 8.6 Hz), 8.29 (1H, s), 7.30 (1H, s), 7.21 (1H, d, *J* = 8.1 Hz), 3.72 (4H, br s), 3.07-2.96 (5H, m), 2.81 (3H, s), 2.70 (3H, s), 1.06 (3H, t, *J* = 7.0 Hz). ^{13}C-NMR (100 MHz, DMSO-D_6) δ: 168.9, 158.7, 157.1, 152.8, 147.5, 142.5, 141.7, 136.1, 130.5, 129.5, 124.4, 123.6, 121.2, 119.2, 52.3, 49.4, 42.4, 41.6, 12.3. HRMS (ESI-TOF) m/z: $[M+H]^+$ Calcd for $C_{22}H_{27}N_6O_3S$ 455.1865; Found 455.1887.

5.1.26. N-(2-isopropoxy-3-(4-methylpiperazine-1-carbonyl)phenyl)-4-oxo-3,4-dihydrothieno [3,2-d]pyrimidine-7-carboxamide (12)

The yield was 59%. White solid. ^{1}H-NMR (400 MHz, $CDCl_3$) δ: 11.39 (1H, s), 8.84 (1H, s), 8.65 (1H, dd, *J* = 8.3, 1.5 Hz), 8.38 (1H, s), 7.19 (1H, dd, *J* = 8.1, 7.3 Hz), 7.07 (1H, dd, *J* = 7.3, 1.5 Hz), 4.45-4.39 (1H, m), 4.10-4.06 (1H, m), 3.72-3.69 (1H, m), 3.50-3.32 (2H, m), 2.62-2.59 (1H, m), 2.50-2.44 (2H, m), 2.35 (3H, s), 2.30-2.28 (1H, m). ^{13}C-NMR (100 MHz, DMSO-D_6) δ: 166.4, 158.6, 157.1, 152.5, 147.8, 142.5, 141.8, 132.6, 130.2, 129.9, 124.5, 123.9, 123.1, 121.2, 76.9, 54.6, 54.1, 46.3, 45.6, 41.0, 22.5, 21.3. HRMS (ESI-TOF) m/z: $[M+H]^+$ Calcd for $C_{22}H_{26}N_5O_4S$ 456.1705; Found 456.1712.

5.2. In vitro TAK1 enzyme assay[16]

To screen TAK1 inhibitors, insect expression vectors against GST-TAK1 and His-TAB1 were infected into insect cells. Then each tag-labeled kinase was purified using an anti-tag antibody-conjugated affinity column. Each purified kinase was mixed and used as an enzyme for screening. The kinase enzyme was incubated with various compounds and subsequently incubated with 6.25 μg of myelin basic protein (Upstate Cat.13-110) and 0.5 μCi of [^{33}P]ATP (3,000 Ci/mmol, GE Healthcare) in 50 μL of the kinase buffer containing 25 mM TBS (pH 7.6), 0.5 mM dithiothreitol, 5 mM $MgCl_2$, 0.0025% Tween20 at 30 °C for 30 min. Then 10 μL of 25% trichloroacetic acid was added into the reaction well and samples were further incubated at 4 °C for 30 min. Acid-precipitated samples were separated by a glass filter and liquid scintillation cocktails were added. The radioactivity of ^{33}P incorporated into myelin basic protein was measured with a MicroBeta (Perkinelmer).

5.3. Liver microsomal stability assay

An aliquot of 1 μM of each compound was incubated with human (or mouse) liver microsome (0.5 mg protein/mL) in 50 mM phosphate buffer (pH 7.4) containing 1 mM NADPH (the reduced form of nicotinamide adenine dinucleotide phosphate) at 37 °C for 30 min. After the enzyme reaction was quenched with the addition of a three-fold volume of acetonitrile, the reaction mixture was centrifuged at 1500 rpm for 10 min. The obtained supernatant was used as a test sample to measure the stability in human (or mouse) liver microsome by measuring the compound in the sample using LC-MS/MS.

5.4. Solubility assay

An aliquot of 50 μL of 1 mM sample in DMSO solution was freeze-dried to remove DMSO. To the resulting residue was added 50 μL of 50 mM phosphate buffer (pH 6.5) or FaSSIF solution, which was then irradiated ultrasonically for 10 min. The solution was shaken for 24 h at 37 °C, centrifuged for 10 min at 25 °C (3000 rpm), and filtered by Whatman Unifilter. Concentration of the filtrate was analyzed by HPLC-UV based on the calibration curve of each sample.

FaSSIF solution was prepared by the following procedure. A solution of L-α-phosphatidylcholine (0.295 g)

and sodium taurocholate (0.805 g) in purified water (5.00 mL) was stirred until the solution was clear. The solution was diluted with purified water (450 mL) and added to KH_2PO_4 (1.95 g) and KCl (3.85g). The pH value of this solution was adjusted to 6.5 by addition of 1N NaOH aq. and diluted with purified water until the volume was 500 mL.

5.5. Expression and purification of TAK1-TAB1 fusion protein for crystallographic structure analysis

The recombinant fusion protein used for crystallization in this study consisted of human TAK1 kinase domain (residue 31-303) and TAB1 (residue 468-504) and was prepared as described previously[29]. Briefly, the truncated version of TAK1 fused to the TAB1 segment incorporated an N-terminal His6 tag and a HRV3c protease cleavage site, and this was inserted into the bacterial/baculoviral expression vector pFastBac1 (Thermo Fisher Scientific). The enzyme was over-expressed in the baculovirus expression system using Sf9 insect cells and then purified from the cell extract using Ni affinity resin (GE Healthcare). Then the N-terminal His6 tag was removed by PreScission protease (GE Healthcare) and the target enzyme was isolated by size-exclusion chromatography on a Superdex 200 26/60 column (GE Healthcare). The resulting sample was loaded onto an anion exchange column (HiTrap-Q HP 5mL, GE Healthcare) that had been equilibrated with 25 mM Tris, pH 8.0, 5 mM DTT, and 10%(v/v) glycerol and was then eluted using a linear gradient of 50–300 mM NaCl. Fractions of the forward peak corresponding to the non-phosphorylated form, as confirmed by SDS-PAGE using Pro-Q Diamond Phosphoprotein Gel Stain (Thermo Fisher Scientific), were pooled and stored at −80 °C for crystallization.

5.6. Crystallization, data collection and structure determination

The purified TAK1-TAB1 fusion protein samples were concentrated to 3 mg/mL with about 0.2 mM of each compound (**10**, **11c** and **12**), and crystallization was carried out by the hanging-drop vapor diffusion method at 20–21 °C. The reservoir solution consisted of 1.7 M sodium potassium phosphate (pH 7.7). Crystals appeared and grew to full size within 4-6 days. These crystals were soaked in a solution of 1.7 M sodium potassium phosphate (pH 7.7) containing 20% glycerol as a cryoprotectant. X-ray diffraction data from crystals of the complex formed from TAK1-TAB1 with ligands **10**, **11c**, or **12** were collected at cryogenic temperatures by the synchrotron radiation sources and detectors shown in Supplementary Table 1.

The diffraction datasets were indexed, integrated, and scaled using the program HKL2000[30] for the complex of TAK1-TAB1 with ligand **10** or **11c**, and using the autoPROC program[31], XDS[32], and Scala[33] for the complex of TAK1-TAB1 with ligand **12**. The structure was determined by molecular replacement with the program MolRep[34] using the published TAK1-TAB1 crystal structure (PDB: 2EVA)[29], as a search model. Models were built with the program Coot[35] and refined with the program Refmac5[36]. The X-ray data collection and refinement statistics are shown in Supplementary Table 1. Refined X-ray coordinates and structure factors of

TAK1-TAB1 in complex with ligands **10**, **11c**, and **12** have been deposited in the PDB with accession codes 5JGB, 5JGA, and 5JGD, respectively.

5.7. Modeling

To calculate the volume of R_2 group of thienopyrimidinone analogs, the initial conformations of R_2 groups were manually modeled by changing R_2 group of **11c** (benzene ring) to each R_2 group. The conformations were optimized in the crystal structure of TAK1/**11c** complex (PDB: 5JGA) by the program Discovery Studio, v4.1 BioVia, San Diego, CA, USA with the TAK1 3D structure fixed. Volume of R_2 group was calculated by using the protocol "Calculate Molecular Properties" of Discovery Studio with the default settings.

Acknowledgments

We thank Y. Itezono for kind advice on NMR measurements, Y. Furuta and M. Arai for HRMS measurements, and Y. Tachibana for kinase panel assay.

Reference and notes

1. Yamaguchi, K.; Shirakabe, K.; Shibuya, H.; Irie, K.; Oishi, I.; Ueno, N.; Taniguchi, T.; Nishida, E.; Matsumoto, K. *Science (New York, N.Y.)* **1995,** *270*, 2008.
2. Sakurai, H. *Trends in pharmacological sciences* **2012,** *33*, 522.
3. Ninomiya-Tsuji, J.; Kishimoto, K.; Hiyama, A.; Inoue, J.; Cao, Z.; Matsumoto, K. *Nature* **1999,** *398*, 252.
4. Sato, S.; Sanjo, H.; Takeda, K.; Ninomiya-Tsuji, J.; Yamamoto, M.; Kawai, T.; Matsumoto, K.; Takeuchi, O.; Akira, S. *Nature immunology* **2005,** *6*, 1087.
5. Shibuya, H.; Yamaguchi, K.; Shirakabe, K.; Tonegawa, A.; Gotoh, Y.; Ueno, N.; Irie, K.; Nishida, E.; Matsumoto, K. *Science (New York, N.Y.)* **1996,** *272*, 1179.
6. Takaesu, G.; Kishida, S.; Hiyama, A.; Yamaguchi, K.; Shibuya, H.; Irie, K.; Ninomiya-Tsuji, J.; Matsumoto, K. *Molecular cell* **2000,** *5*, 649.
7. Ishitani, T.; Takaesu, G.; Ninomiya-Tsuji, J.; Shibuya, H.; Gaynor, R. B.; Matsumoto, K. *The EMBO journal* **2003,** *22*, 6277.
8. Adcock, I. M.; Chung, K. F.; Caramori, G.; Ito, K. *European journal of pharmacology* **2006,** *533*, 118.
9. Courties, G.; Seiffart, V.; Presumey, J.; Escriou, V.; Scherman, D.; Zwerina, J.; Ruiz, G.; Zietara, N.; Jablonska, J.; Weiss, S.; Hoffmann, A.; Jorgensen, C.; Apparailly, F.; Gross, G. *Blood* **2010,** *116*, 3505.
10. Kumar, R.; Crouthamel, M. C.; Rominger, D. H.; Gontarek, R. R.; Tummino, P. J.; Levin, R. A.; King, A. G. *British journal of cancer* **2009,** *101*, 1717.

11. Izzedine, H.; Rixe, O.; Billemont, B.; Baumelou, A.; Deray, G. *American journal of kidney diseases : the official journal of the National Kidney Foundation* **2007,** *50*, 203.

12. Gilliland, D. G.; Griffin, J. D. *Blood* **2002,** *100*, 1532.

13. Manning, G.; Whyte, D. B.; Martinez, R.; Hunter, T.; Sudarsanam, S. *Science (New York, N.Y.)* **2002,** *298*, 1912.

14. Kilty, I.; Jones, L. H. *Future medicinal chemistry* **2015,** *7*, 23.

15. Wu, J.; Powell, F.; Larsen, N. A.; Lai, Z.; Byth, K. F.; Read, J.; Gu, R. F.; Roth, M.; Toader, D.; Saeh, J. C.; Chen, H. *ACS chemical biology* **2013,** *8*, 643.

16. Ninomiya-Tsuji, J.; Kajino, T.; Ono, K.; Ohtomo, T.; Matsumoto, M.; Shiina, M.; Mihara, M.; Tsuchiya, M.; Matsumoto, K. *The Journal of biological chemistry* **2003,** *278*, 18485.

17. Kamiyama, H.; Usui, T.; Sakurai, H.; Shoji, M.; Hayashi, Y.; Kakeya, H.; Osada, H. *Bioscience, biotechnology, and biochemistry* **2008,** *72*, 1894.

18. Kamiyama, H.; Kakeya, H.; Usui, T.; Nishikawa, K.; Shoji, M.; Hayashi, Y.; Osada, H. *Oncology research* **2008,** *17*, 11.

19. Byth, K.; Palakurthi, S.; Yu, L.; Zhang, Q.; **2008**.

20. Lockman, J. W.; Reeder, M. D.; Robinson, R.; Ormonde, P. A.; Cimbora, D. M.; Williams, B. L.; Willardsen, J. A. *Bioorganic & medicinal chemistry letters* **2011,** *21*, 1724.

21. Buglio, D.; Palakurthi, S.; Byth, K.; Vega, F.; Toader, D.; Saeh, J.; Neelapu, S. S.; Younes, A. *Blood* **2012,** *120*, 347.

22. Hornberger, K. R.; Berger, D. M.; Crew, A. P.; Dong, H.; Kleinberg, A.; Li, A. H.; Medeiros, M. R.; Mulvihill, M. J.; Siu, K.; Tarrant, J.; Wang, J.; Weng, F.; Wilde, V. L.; Albertella, M.; Bittner, M.; Cooke, A.; Gray, M. J.; Maresca, P.; May, E.; Meyn, P.; Peick, W., Jr.; Romashko, D.; Tanowitz, M.; Tokar, B. *Bioorganic & medicinal chemistry letters* **2013,** *23*, 4517.

23. Hornberger, K. R.; Chen, X.; Crew, A. P.; Kleinberg, A.; Ma, L.; Mulvihill, M. J.; Wang, J.; Wilde, V. L.; Albertella, M.; Bittner, M.; Cooke, A.; Kadhim, S.; Kahler, J.; Maresca, P.; May, E.; Meyn, P.; Romashko, D.; Tokar, B.; Turton, R. *Bioorganic & medicinal chemistry letters* **2013,** *23*, 4511.

24. Kilty, I.; Green, M. P.; Bell, A. S.; Brown, D. G.; Dodd, P. G.; Hewson, C.; Hughes, S. J.; Phillips, C.; Ryckmans, T.; Smith, R. T.; van Hoorn, W. P.; Cohen, P.; Jones, L. H. *Chemical biology & drug design* **2013,** *82*, 500.

25. Arora, N.; Chen, S.; Hermann, J. C.; Kuglstatter, A.; Labadie, S. S.; Lin, C. J. J.; Lucas, M. C.; Moore, A. G.; Papp, E.; Talamas, F. X.; Wanner, J.; Zhai, Y.; **2012**.

26. Ishikawa, M.; Hashimoto, Y. *Journal of medicinal chemistry* **2011,** *54*, 1539.

27. Nishio, M.; Umezawa, Y.; Fantini, J.; Weiss, M. S.; Chakrabarti, P. *Physical*

chemistry chemical physics : PCCP **2014,** *16*, 12648.

28. Griffith, J.; Black, J.; Faerman, C.; Swenson, L.; Wynn, M.; Lu, F.; Lippke, J.; Saxena, K. *Molecular cell* **2004,** *13*, 169.

29. Brown, K.; Vial, S. C.; Dedi, N.; Long, J. M.; Dunster, N. J.; Cheetham, G. M. *Journal of molecular biology* **2005,** *354*, 1013.

30. Otwinowski, Z.; Minor, W. In *Methods in Enzymology*; Academic Press, 1997; Vol. Volume 276, pp. 307.

31. Vonrhein, C.; Flensburg, C.; Keller, P.; Sharff, A.; Smart, O.; Paciorek, W.; Womack, T.; Bricogne, G. *Acta crystallographica. Section D, Biological crystallography* **2011,** *67*, 293.

32. Kabsch, W. *Acta crystallographica. Section D, Biological crystallography* **2010,** *66*, 125.

33. Evans, P. *Acta crystallographica. Section D, Biological crystallography* **2006,** *62*, 72.

34. Vagin, A.; Teplyakov, A. *Acta crystallographica. Section D, Biological crystallography* **2010,** *66*, 22.

35. Emsley, P.; Lohkamp, B.; Scott, W. G.; Cowtan, K. *Acta crystallographica. Section D, Biological crystallography* **2010,** *66*, 486.

36. Gruene, T. *Acta crystallographica. Section D, Biological crystallography* **2013,** *69*, 1861.

*Graphical Abstract (for review)

structure based drug design

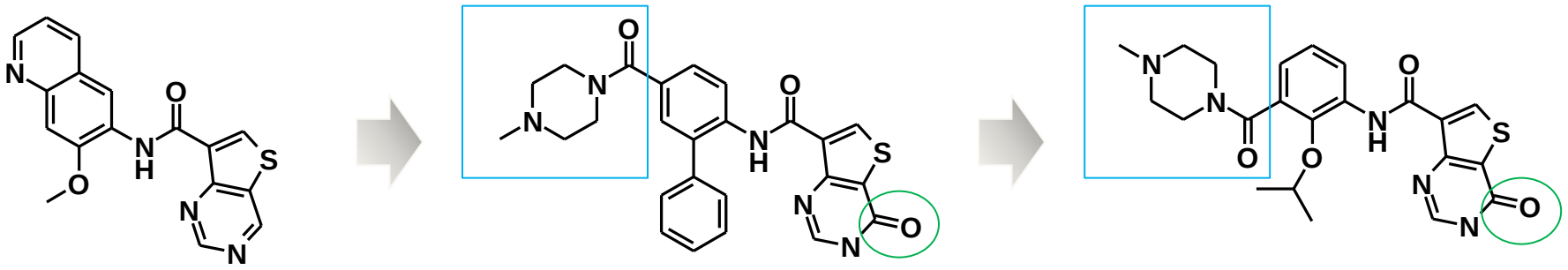

Metabolic identification

Hit compound
TAK1 inhibitory activity
37% inhibition@1μM

TAK1 IC_{50} = 2.3 nM
Low kinase selectivity

TAK1 IC_{50} = 11 nM
high kinase selectivity